Using Impedance Flow Cytometry for Rapid Viability Classification of Heat-Treated Bacteria

Bertelsen, Christian Vinther; Skands, Gustav Erik; González Díaz, Marcos; Dimaki, Maria; Svendsen, Winnie Edith

Published in:
ACS Omega

Link to article, DOI:
10.1021/acsomega.2c07357

Publication date:
2023

Document Version
Publisher's PDF, also known as Version of record

ACS OMEGA

http://pubs.acs.org/journal/acsodf

Article

Using Impedance Flow Cytometry for Rapid Viability Classification of Heat-Treated Bacteria

Christian Vinther Bertelsen,* Gustav Erik Skands, Marcos González Díaz, Maria Dimaki, and Winnie Edith Svendsen

Cite This: *ACS Omega* 2023, 8, 7714−7721

Read Online

ACCESS | Metrics & More | Article Recommendations | Supporting Information

ABSTRACT: In the future, rapid electrical characterization of cells with impedance flow cytometry promises to be a fast and accurate method for the evaluation of cell properties. In this paper, we investigate how the conductivity of the suspending medium along with the heat exposure time affects the viability classification of heat-treated *E. coli*. Using a theoretical model, we show that perforation of the bacteria membrane during heat exposure changes the impedance of the bacterial cell from effectively less conducting than the suspension medium to effectively more conducting. Consequently, this results in a shift in the differential argument of the complex electrical current that can be measured with impedance flow cytometry. We observe this shift experimentally through measurements on *E. coli* samples with varying medium conductivity and heat exposure times. We show that increased exposure time and lower medium conductivity results in improved classification between untreated and heat-treated bacteria. The best classification was achieved with a medium conductivity of 0.045 S/m after 30 min of heat exposure.

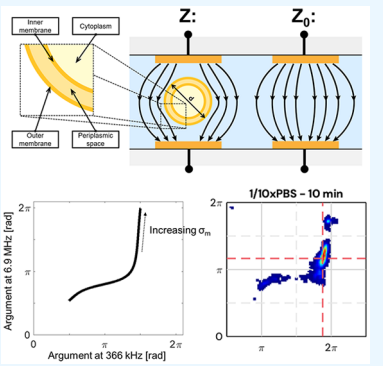

INTRODUCTION

Impedance flow cytometry (IFC) has seen significant interest and investigation in the last 2 decades[1−3] due to its potential for label-free characterization of biological cells and its simple process for fabrication of chips. In impedance flow cytometry, a liquid containing particles or cells is continuously injected and flows across a set of detection electrodes. The change in current during the passing of a particle is measured simultaneously at multiple frequencies and, as result, different parts of the cell structure are probed.

The majority of IFC related work has focused on characterization of larger cells such as red blood cells, yeast, and other eukaryotic cells.[4−9] Less work has gone into investigating bacteria and other smaller particles, likely because it is difficult to achieve sufficient signal-to-noise ratios for smaller cells. Multiple studies have tried to suggest changes to the design and fabrication of the detection electrodes meant to improve the sensitivity of the technology.[10−15] However, the bacteria studies that have been done have focused on simple detection and differentiation from nonbiological particles,[16−18] and on the assessment of the viability of the bacteria.[19−21]

Previously, we have looked into the effect of three inactivation methods on the IFC characterization of *E. coli*.[22] To do that, we inactivated the bacteria using ethanol, autoclaving, and heat exposure (90 °C). We further investigated the viability of the cells before and after inactivation using three methods: plate counts on agar plates, membrane integrity using a fluorescent viability kit, and impedance flow cytometry (using a prototype impedance flow cytometer from the Danish company SBT Instruments A/S). The plate counts confirmed the inactivation (i.e., no growth) for all three inactivation methods, and the investigation with the fluorescent viability kit showed that the membranes of the bacterial cells were perforated after inactivation. Surprisingly, however, we found that the impedance response was different after inactivation for the three inactivation methods. While cells inactivated with either ethanol or with autoclaving could be classified as such with a selectivity of 99.6% and 90.9% compared to viable cells, cells inactivated by heat (90 °C) could only be classified with a selectivity of 18.0% compared to untreated cells. This left a fascinating unanswered question about why heat inactivated bacteria, that show no growth on appropriate agar plates and have perforated membranes, do not exhibit a significant change in impedance response.

In this paper, we describe our latest investigations of the impedance response of bacterial cells after heat inactivation. We attempt to clarify how the duration of the heat exposure affects the IFC results. We investigate if prolonged exposure to heat (at 90 °C) affects the ability of IFC to classify heat-treated cells from untreated cells, again using an impedance flow cytometry prototype from SBT Instruments. We also examine

Received: November 16, 2022
Accepted: February 3, 2023
Published: February 16, 2023

https://doi.org/10.1021/acsomega.2c07357
ACS Omega 2023, 8, 7714−7721

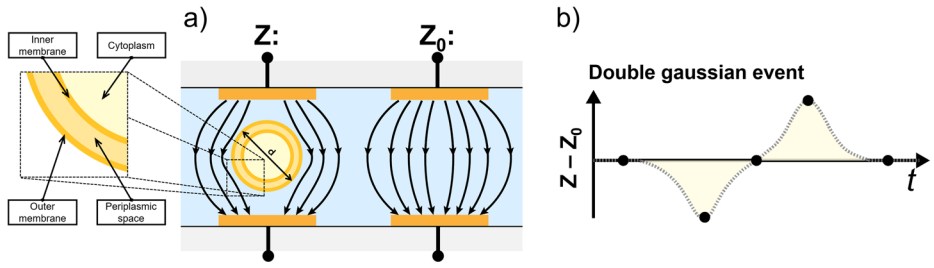

Figure 1. Dielectric bacteria modeling. (a) Sketch showing a microfluidic channel with two sets of front-facing microelectrodes. A bacterium represented as a sphere with diameter, d, and three concentric shells around it, is located between the first set of electrodes. The shells represent the outer membrane, periplasmic space, and inner membrane of the cell. (b) Characteristic double Gaussian event that forms in the differential impedance $(Z - Z_0)$ when the bacterium transitions sequentially between the two electrodes sets.

what role the conductivity of the suspension media plays in the effectiveness of the classification. We attempt to explain the observed behavior using an analytical model based on Maxwell mixture theory.

THEORY

Impedance measurements of cells has been used for almost a hundred years to study the viability of cells and cell cultures.[23] The prevailing idea is that the inactivation method perforates the lipid membrane of the cell, leading to a breakdown of metabolic activity and an inability of the cell to maintain structure.[24,25]

This is especially true for eukaryotic cells, but also cells with more rigid envelope structures are considered nonviable when the lipid membrane is broken.[24] For a healthy cell, an intact membrane acts as an insulating barrier surrounding the cytoplasm in the core of the cell. More specifically, the insulating membrane acts as a capacitor that electrically shields the cell interior at lower frequencies (typically <1 MHz) but is short circuited at higher frequencies (typically >1 MHz)[26,27] making way for electrically probing of the membrane and cell interior.[28] This idea is also the basis of several commercially available cell counters based on the Coulter counter principle.[29]

Bacteria are not homogeneous particles but are often represented by more or less complex models of concentric shells (i.e., the cell envelope) around a homogeneous interior (i.e., the cytoplasm of the cell). Since we are performing the IFC experiments on samples with Gram-negative *E. coli* bacteria, we have chosen to represent the bacteria as a spherical model with three shells representing the three layers found in the cell envelope structure of Gram-negative bacteria: the outer membrane, the periplasmic space, and the inner membrane (or plasma membrane), as shown in the inset of Figure 1a. More complex modeling of the bacteria shape can be done (e.g., elongated shape[30]); however, spherical modeling is sufficient to describe the general behavior of the impedance. The impedance chips used for the experiments have two sets of front-facing microelectrodes as illustrated in Figure 1a. As the bacteria transitions through the microchannel and sequentially passes between the two sets of electrodes, the corresponding differential impedance forms a characteristic double Gaussian shown in Figure 1b. The peak value of the transition corresponds to the situation where the cell is between one of the electrode sets. In the following, we will refer to the peak impedance between the first electrode set (with the bacterium) as Z and the impedance of the second electrode (without the bacterium) set as Z_0.

We use Maxwell mixture theory to predict the impedance behavior of inactivated cells (i.e., cells with perforated membranes). To do this, we will use the complex permittivity that depends on the relative permittivity (ε), the conductivity (σ), and the angular frequency (ω) in the following way:

$$\varepsilon^* = \varepsilon - j\frac{\sigma}{\omega} \tag{1}$$

For a nonhomogeneous shelled sphere like the one used to represent the Gram-negative bacterium, an effective complex permittivity (ε^*_{eff}) can be calculated that takes the combined electrical properties of the interior of the cell (ε_i^*) and each of the shells into account.[31] This complex permittivity can be calculated by first calculating the effective permittivity of the interior sphere with one shell and then continually adding additional shells starting from the innermost one:

$$\varepsilon^*_{eff} = \frac{\left(\frac{d/2}{d/2 - d_{shell}}\right)^3 + 2\left(\frac{\varepsilon_i^* - \varepsilon^*_{shell}}{\varepsilon_i^* + 2\varepsilon^*_{shell}}\right)}{\left(\frac{d/2}{d/2 - d_{shell}}\right)^3 - \left(\frac{\varepsilon_i^* - \varepsilon^*_{shell}}{\varepsilon_i^* + 2\varepsilon^*_{shell}}\right)} \tag{2}$$

The effective permittivity of the bacteria suspended in the electrolyte medium (ε^*_{mix}) is given by the Maxwell-Garnett mixing equation:[32,33]

$$\frac{\varepsilon^*_{mix} - \varepsilon^*_m}{\varepsilon^*_{mix} + 2\varepsilon^*_m} = \phi\frac{\varepsilon^*_{eff} - \varepsilon^*_m}{\varepsilon^*_{eff} + 2\varepsilon^*_m} \Rightarrow \varepsilon^*_{mix} = \varepsilon^*_m\frac{1 + 2\phi\frac{\varepsilon^*_{eff} - \varepsilon^*_m}{\varepsilon^*_{eff} + 2\varepsilon^*_m}}{1 - \phi\frac{\varepsilon^*_{eff} - \varepsilon^*_m}{\varepsilon^*_{eff} + 2\varepsilon^*_m}} \tag{3}$$

where ϕ is the volume fraction occupied by the bacterial cell (see Supporting Information) and (ε^*_{mix}) is the complex permittivity of the medium.

The differential complex impedance of the entire system $(\Delta Z = Z - Z_0)$ can then be calculated using eqs 4 and 5:

$$Z^* = \frac{1}{j\omega\varepsilon^*_{mix} l\kappa} \tag{4}$$

$$Z_0^* = \frac{1}{j\omega\varepsilon^*_m l\kappa} \tag{5}$$

with κ being a correction factor (see Supporting Information) for the nonuniformity of the electric field at the electrode edges into account[2,34] that depends on the width of the electrodes in the direction of the flow and the height of the detection channel, and l is the length of the electrode perpendicular to the flow. Using Ohms law, the current (I^*) and subsequently the differential current (ΔI^*) can be calculated:

https://doi.org/10.1021/acsomega.2c07357
ACS Omega 2023, 8, 7714−7721

Table 1. Dielectric Properties and Thickness of the Three Shells (Outer Membrane, Periplasmic Space, Inner Membrane) and the Interior Core (Cytoplasm) Used for Modeling of the Bacterium[a]

	outer membrane	periplasmic space	inner membrane	cytoplasm	media
conductivity (σ) [mS/m]	1e−1	3200	1e−6	220	40
					80
					160
					800
permittivity (ε)	12.1	60	5.5	108	80
thickness [nm]	8	15	4	not applicable	not applicable

[a]Dielectric properties from ref 36, media properties from experimental parameters.

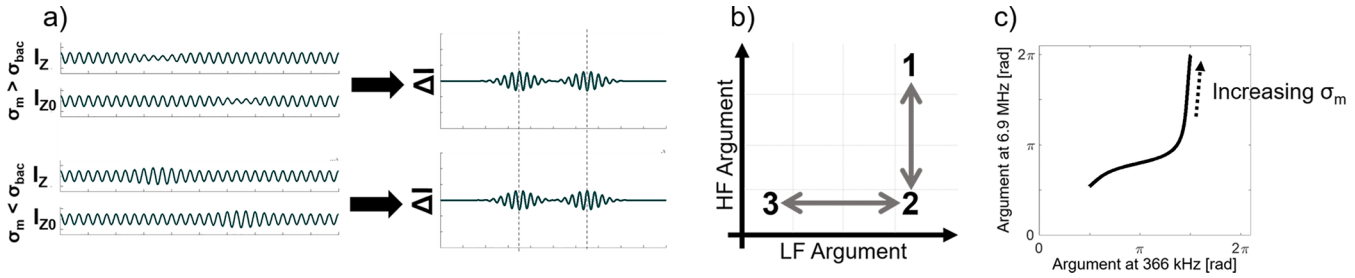

Figure 2. Influence of relative conductivity. (a) Sketch of the time dependent AC current (one frequency) on two electrode sets during the passage of a particle/bacterium with a lower effective conductivity than the medium surrounding it ($\sigma_{bac} < \sigma_m$) and the reverse situation where the particle/bacterium has a higher effective conductivity compared to the medium ($\sigma_{bac} > \sigma_m$). (b) Sketch of the 3 main proposed positions of particles/bacteria populations in a scatterplot with argument at low frequency on the x-axis and the argument of the high frequency on the y-axis. In position 1, the impedance of the particles/bacteria are effectively higher than that of the surrounding medium at both low and high frequency (e.g., homogeneous nonconducting beads). In position 2, the impedance of the particles/bacteria in the high frequency is lower than that of the medium (e.g., bacteria cells with intact membranes if the high frequency is high enough to bypass the membrane capacitance). In position 3, the particles/bacteria are effectively more conducting than the medium at both frequencies (e.g., cells with broken membranes). (c) Analytical calculation based on MMT that shows the behavior of a bacteria with fixed properties in a medium with increasing conductivity. The bacteria position follows the predicted positions as the media conductivity increases (i.e., as the bacteria moves from more conducting to less conducting than the medium).

$$I^* = \frac{U}{Z^*} \tag{6}$$

$$\Delta I^* = I^* - I_0^* \tag{7}$$

The differential modulus and argument can then be calculated using

$$\mathrm{mod}(\Delta I^*) = |\Delta I^*| = \sqrt{\mathrm{re}(\Delta I^*)^2 + \mathrm{im}(\Delta I^*)^2} \tag{8}$$

$$\arg(\Delta I^*) = \mathrm{atan}\,2(\mathrm{re}(\Delta I^*),\ \mathrm{im}(\Delta I^*)) \tag{9}$$

The cell properties of the bacteria depend on factors such as strain and growth conditions.[35] For modeling, we use electrode dimensions of 10 μm width and 25 μm in length and a channel height of 10 μm identical to the dimension of the chip used for experiments. The applied voltage (U) is 16 V_{pp} combined for both frequencies and the bacteria diameter is 1 μm with the dielectric properties of the shells and interior found in Table 1.

Usually, IFC experiments are carried out using medium with relatively high conductivity (e.g., 1xPBS at ∼1.6 S/m) compared to the cells that are probed. This is overall a good strategy since it usually leads to higher current and better signal-to-noise ratio (i.e., peak-to-noise).[36]

However, we conduct our experiments using phosphate buffered saline (PBS) diluted with ultrapure water (UPW) to lower the conductivity of the PBS. While this does affect the peak-to-noise ratio, it also leads to a situation where the differential argument of the current depends heavily on whether the bacterium increases or decreases the impedance of the system during a transition. More specifically, the differential current shifts out of phase if the cell changes from being effectively less conducting to effectively more conducting than the medium and vice versa. If the original signals that are subtracted are in phase, the resulting differential phase will shift from in-phase to out-of-phase when the amplitude of one of the signals changes from larger to smaller than the other signal. This idea is illustrated in Figure 2 for situations where the bacteria is less conducting than the medium and more conducting than the medium.

For bacteria, measurements with IFC various conditions determine if this shift happens, for example, when changing the frequency from a low frequency where the membrane blocks the current and the impedance is high, to a higher frequency where the membrane is more transparent to the current, and the impedance is lowered (on the condition that the conductivity of the cell interior is higher than that of the media). Additionally, the phase shift will also occur at lower frequencies when the membrane of the cell is perforated, e.g., after inactivation. As the membrane perforates, the effective impedance of the membrane drops, and the cell interior is probed even at lower frequencies.

For cell measurements, the two subtracted signals are not necessarily completely in-phase due to the capacitance of the system (primarily from the lipid membrane). Even so, when plotting the differential argument, the detected events are expected to move between three general positions as indicated in Figure 2b:

- Position 1: The cells/particles are effectively less conducting than the medium at both low and high frequency ($|Z| > |Z_0|$). This could be e.g., polystyrene beads.

https://doi.org/10.1021/acsomega.2c07357
ACS Omega 2023, 8, 7714−7721

- Position 2: The cells/particles are effectively less conducting than the medium at the low frequency ($|Z| > |Z_0|$), but more conducting in the high frequency ($|Z| < |Z_0|$). This could be, e.g., cells with intact cell membranes that are opaque at low frequencies but transparent at high frequencies
- Position 3: The cells/particles are effectively more conducting than the medium at both low and high frequency ($|Z| < |Z_0|$). This could be, e.g., cells with broken membranes that allow current to run through the more conducing cell interior, even at low frequencies.

Whether the bacteria are more or less conducting compared to the surrounding media obviously depends on the conductivity of the medium. In Figure 2c, the differential argument calculated using the model properties found in Table 1 is plotted with increasing medium conductivity for the two frequencies used for experiments (366 kHz and 6.9 MHz). As the medium conductivity increases, it is seen that the predicted differential argument passes through the 3 positions as the cells go from being more conducting to less conducting than the medium.

In Figure 3, the differential phase as a function of inner and outer membrane conductivity is plotted for the two experimental frequencies (366 kHz and 6.9 MHz) and changing medium conductivities (40 mS/m, 80 mS/m, 160 mS/m, and 800 mS/m). We see that the conductivity of both membranes can increase multiple orders of magnitude before the shift occurs and that the shift does not happen if the medium conductivity is higher than the cytoplasm conductivity (here 220 mS/m). This tells us that it is not just a matter of "if" the membrane is perforated, but also the degree of perforation and that a perforated membrane in itself is not enough to differentiate inactivated cells from intact cells based on differential argument.

The analytical results lead to the following expectations for the experimental results:

- A shift in the argument means that the membrane is perforated enough, so that the effective conductivity of the cell is higher than that of the surrounding media.
- It is not necessary that both outer and inner membranes are perforated if the conductivity of the periplasm is high enough. In this way, the cell becomes effectively more conducting than the media surrounding it even if only the outer membrane is perforated.
- The shift in argument is expected to happen "sooner" (i.e., at lower membrane conductivities) when the media conductivity is lower.
- If the argument does not shift, it means that the membrane is not sufficiently perforated or that the conductivity of the cell interior is lower than that of the surrounding media.
- The shift in argument is expected to be more significant in the low frequency compared to the high frequency.

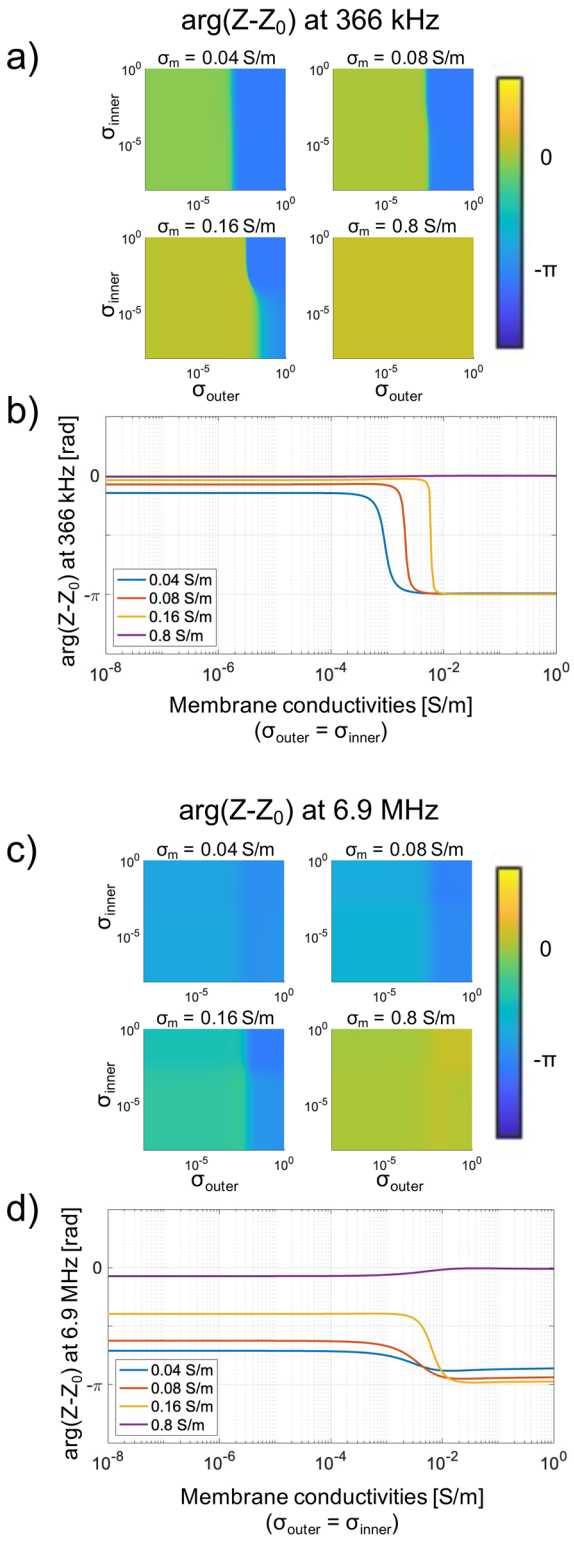

Figure 3. Differential argument as a function of membrane conductivity. Color gradient map of the calculated differential argument for increasing conductivity of the inner and outer membrane (σ_{inner}, σ_{outer}) at the experimental frequencies of (a) 366 kHz and (c) 6.9 MHz at 4 different medium conductivities (σ_m): 40 mS/m, 80 mS/m, 160 mS/m, and 800 mS/m. (b, d) Differential argument at the diagonal line ($\sigma_{inner} = \sigma_{outer}$) of the color gradient maps for each of the conductivities.

METHODS

Testing the Effects of Prolonged Heat Exposure. Preparation of heat inactivated samples were performed in order to duplicate results from our previous work.[22] *E. coli* bacteria (ATCC8739) were grown overnight in TSB (tryptic soy broth, Sigma-Aldrich) at 37 °C and with 180 rpm shaking. The following day, 10 μL of the overnight culture was transferred to a vial with 10 mL of fresh TSB and incubated for 5 h. Five glass vials, each containing 1 mL of culture, were then prepared. Four of them were placed inside an aluminum heat

https://doi.org/10.1021/acsomega.2c07357
ACS Omega 2023, 8, 7714−7721

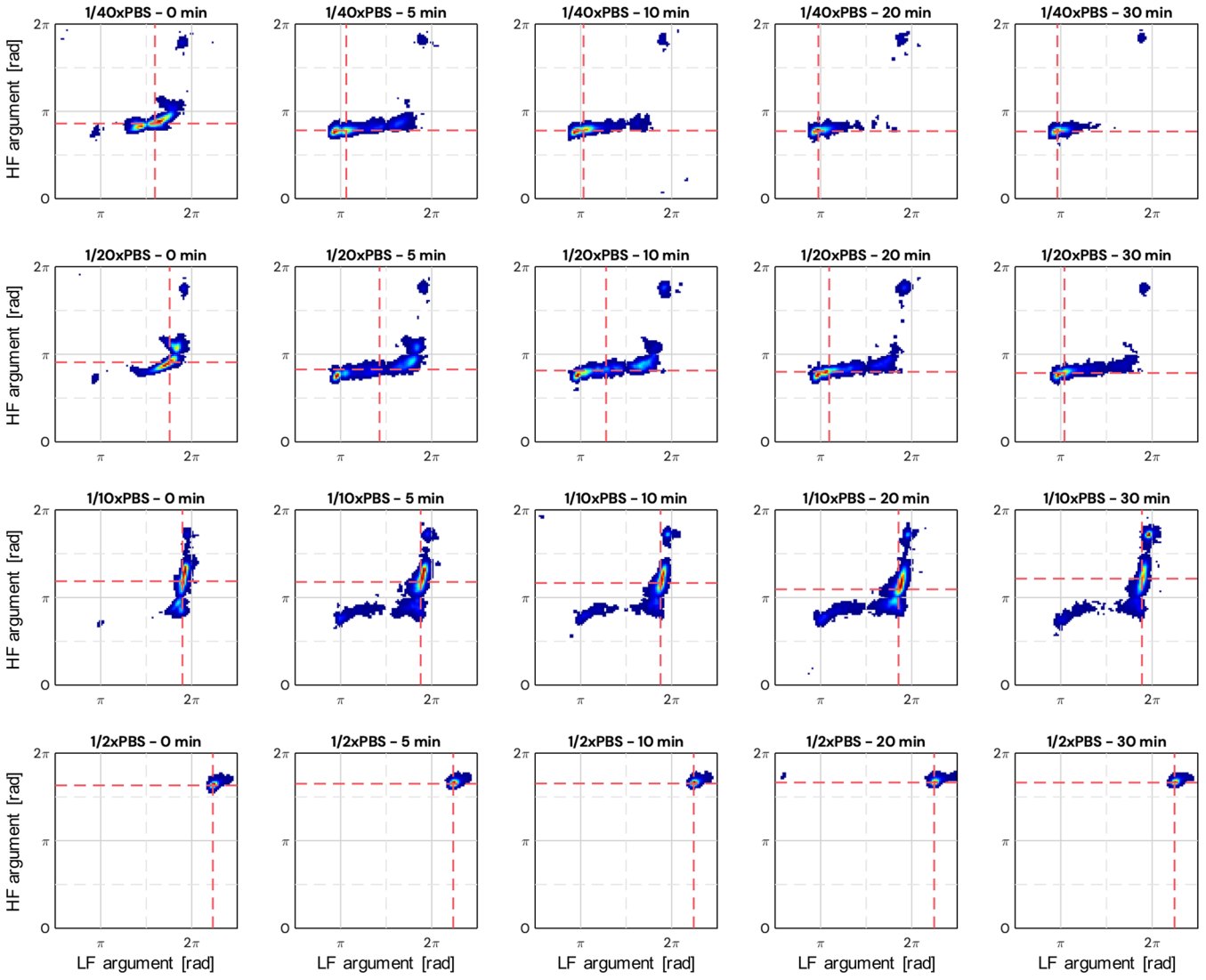

Figure 4. Density plots of experimental results. Density plots showing the results from individual measurements on samples with increasing heat exposure times (0 to 30 min in columns left to right) and medium conductivity (1/40xPBS to 1/2xPBS in rows top to bottom). Striped, red lines indicate the median value of the LF and HF argument for each population.

block on a hot plate. The hot plate was set to 90 °C, and the temperature of the block was monitored using a thermometer submerged in an ultrapure water (UPW) sample also placed in the heat block.

One bacteria sample was placed directly on ice, while the subsequent 4 samples were removed from the heat block after 5, 10, 20, and 30 min and then placed on ice.

Drop plating (3 drops of 10 μL on tryptic soy agar) was used to confirm the inactivation was successful so that no cell growth was observed after 24 h in any of the heat-treated samples.

For IFC measurements, 3 μL of bacteria sample was transferred into 3 mL (1/1000 dilution) of diluted PBS (Dulbecco's phosphate buffered saline, Sigma-Aldrich). This is done to reduce both the concentration of cells in the sample and the conductivity contribution from the growth media. The PBS was diluted with UPW in the following ratios: 1/40, 1/20, 1/10, and 1/2. The UPW is deionized, and the conductivity of the sample is therefore dependent on the dilution of the PBS. The conductivity of the 4 samples was measured using a Primo5 conductivity meter (HannaNorden AB, Sweden) to be 45 mS/m, 85 mS/m, 175 mS/m, and 860 mS/m, respectively.

IFC Measurements. The IFC measurements were carried out using an impedance flow cytometer prototype from SBT Instruments A/S (Herlev, Denmark). Each sample was measured using the IFC prototype at two simultaneous frequencies of 366 kHz and 6.9 MHz to match the previously obtained results.[22] The voltage applied to the electrode was 15 V_{pp} for all samples except for the samples in 1/2xPBS where it was reduced to 1.5 V_{pp} to avoid clipping of the differential signal at the ADC. The clipping of the signal happens because of asymmetries in the detection electrode fabrication that causes the differential current between the electrode sets (Z and Z_0) to be different from 0. As the medium conductance is increased this nonzero current increases beyond the dynamic range of the ADC in the flow cytometer. To mitigate this, the input voltage is reduced leading to a reduction in peak height of the events. Because the argument is calculated as the ratio of imaginary and real part of the signal, a reduction in peak height does not affect it, but obviously the moduli cannot be compared without some form of normalization.

https://doi.org/10.1021/acsomega.2c07357
ACS Omega 2023, 8, 7714−7721

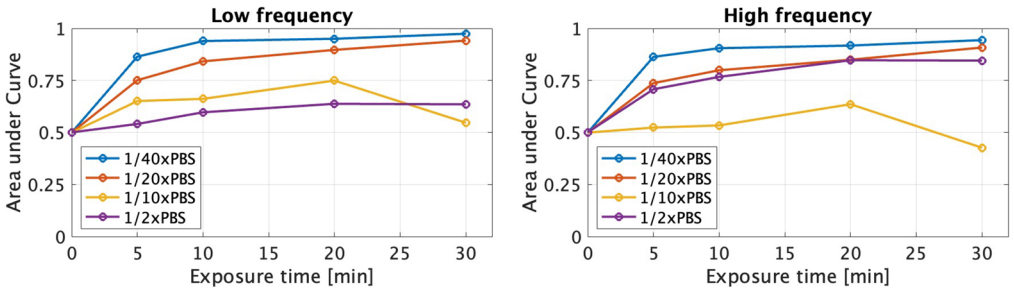

Figure 5. Area under curve. AUC values as a function of exposure time for low and high frequency (366 kHz and 6.9 MHz). For each exposure time, the AUC for samples with conductivities of 1/40xPBS, 1/20xPBS, 1/10xPBS, and 1/2xPBS is plotted. An AUC value of 0.5 indicates that classification is not possible, while an AUC of 1 means perfect classification.

The raw IFC measurements were analyzed using a custom software program created by SBT Instruments. The results were plotted as density plots (based on kernel density estimation) showing the differential argument for low and high frequency. Furthermore, ROC curves were generated using MATLAB to show how well the heat inactivated cells can be differentiated from untreated cells.

RESULTS AND DISCUSSION

No cell growth was seen on any of the heat exposed samples after 24 h at 37 °C, meaning that the *E. coli* are inactivated after 5 min of exposure to 90 °C.

Impedance Response of Heat-Treated *E. coli*. Figure 4 shows the measured differential argument of the impedance at 366 kHz and 6.9 MHz. The figure shows a grid of plots, each plot based on a measurement with a specific heat exposure time and medium conductivity. The exposure time increases with each row from leftmost (0 min, i.e., untreated) to rightmost (30 min). Similarly, measurements with low conductivity medium (1/40xPBS) are found in the top row, with increasing conductivity for the rows below, ending at 1/2xPBS at the bottom row. The low-density populations of events seen in almost all samples at position 1 and position 3 are expected to be cell residues and/or debris from the flow system (from tubing, pumps, etc.). These populations are observed even in pure PBS samples.

The interplay between the exposure time, medium conductivity, and the movement of the measured population between the three general positions is seen in Figure 4.

When the surrounding media conductivity is low (i.e., 1/40xPBS and 1/20xPBS), the differential argument shifts when the heat exposure time increases and more of the cells shift from position 2 toward position 3. This supports the idea that prolonged exposure to heat further breaks down the cell membrane and allows current to pass through the bacterium at the low frequency, effectively shifting the cell from being less conducting to more conducting than the medium surrounding it.

It also supports the prediction that simple perforation is not enough to shift the population but that the effective conductivity of the membrane must change several orders of magnitude before the shift happens (e.g., longer exposure causes larger or additional ruptures in the membrane).

Remember that the bacteria cells in the samples do not grow, so it is not a question of whether the additional perforation inactivates the cell. The important point is that the perforation becomes more apparent in the impedance signal as the population shifts more for increased exposure times.

As the media conductivity increases (1/10xPBS and 1/2xPBS), the shift in differential argument is not apparent. For the sample 1/10xPBS, we see that some cells shift when going from untreated cells to heat inactivated cells, but most of the cells stay in the same position. We only expect the relative impedance to change if the conductivity of the cell interior is higher than that of the medium and these results therefore indicate that the cytoplasm conductivity is at or below that of 1/10xPBS (~160 mS/m). This may be an underestimation since exchange between cytoplasm and medium could occur as the membrane perforates artificially lowering the cytoplasm conductivity. However, if the cytoplasm was fully replaced by medium, we would not expect to see a shift in population at the lower medium conductivities.

Classification of Viable and Inactivated Bacteria. Differentiation between untreated and heat-treated cells is done by generating ROC curves and calculating the area-under-curve (AUC). A higher AUC is an indication of better classification while an AUC of 0.5 means the classification is no better than random. The calculated AUC based on the low and high frequency argument as a function of exposure time can be seen in Figure 5. They show that the classification between heat-treated and untreated *E. coli* improves as the exposure time is extended, as well as for lower medium conductivities. The ROC curves themselves can be seen in the Supporting Information (Figure S1).

From Figure 5, we can see that the best classification between untreated and heat-treated bacteria is achieved when classifying based on the low frequency argument for the bacteria that have been exposed to the heat for 30 min (although the improvement from 10 to 30 min is not very large) and are suspended in the lowest conductivity medium (1/40xPBS). It is reasonable that the best classification is seen in the low frequency since the relative change in membrane impedance is larger going from an intact and "opaque" membrane to a perforated one. Under these conditions, a simultaneous sensitivity of 97.1% (ratio of untreated bacteria correctly classified as such) and a selectivity of 99.1% (ratio of heat-treated bacteria correctly classified as such) can be achieved. This is a noticeable improvement compared to our previous work, where the optimal threshold (found in the high frequency argument) only yielded a selectivity of 18.0%. A surprising observation was the decrease in the AUC for 30 min heat exposure in 1/10xPBS. It is currently unknown if this drop is related to the heat resistance of the bacteria or to experimental variations.

https://doi.org/10.1021/acsomega.2c07357
ACS Omega 2023, 8, 7714−7721

CONCLUSION

In this paper, we have presented our measurements on heat treated *E. coli* bacteria using impedance flow cytometry. We have shown that the bacteria can be classified based on whether they are heat-treated but that the performance of the classification depends on the duration of the heat exposure and the conductivity of the medium. The impedance classification relies on a shift in the differential argument of the bacteria that occurs when the bacterial cell changes from being less conducting to more conducting than the medium surrounding it. This seems to depend not only on the medium conductivity but also on the duration of the heat exposure step, indicating that the structural changes in the bacteria membrane during heating may also be time dependent. We found the best differentiation between untreated and heat-treated *E. coli* when the sample was heat-treated for 30 min and was suspended in a medium with a conductivity of 45 mS/m (1/40xPBS). However, the relevance of these particular conditions may change depending on the investigated strain and application. What remains clear is that care must be taken when using impedance flow cytometry to classify the viability state of heat-treated *E. coli*. Further studies should be conducted to understand how the cell structure changes during prolonged heat treatment and correlated to the observed change in impedance.

ASSOCIATED CONTENT

Supporting Information

The Supporting Information is available free of charge at https://pubs.acs.org/doi/10.1021/acsomega.2c07357.

Theory; ROC curves; FPGA error (PDF)

AUTHOR INFORMATION

Corresponding Author

Christian Vinther Bertelsen − *DTU Bioengineering, Technical University of Denmark, 2800 Kgs Lyngby, Denmark; SBT Instruments A/S, 2730 Herlev, Denmark;* orcid.org/0000-0001-6159-0559; Email: cvbe@dtu.dk

Authors

Gustav Erik Skands − *SBT Instruments A/S, 2730 Herlev, Denmark*

Marcos González Díaz − *SBT Instruments A/S, 2730 Herlev, Denmark*

Maria Dimaki − *DTU Bioengineering, Technical University of Denmark, 2800 Kgs Lyngby, Denmark*

Winnie Edith Svendsen − *DTU Bioengineering, Technical University of Denmark, 2800 Kgs Lyngby, Denmark*

Complete contact information is available at: https://pubs.acs.org/10.1021/acsomega.2c07357

Funding

This research is partially funded by Innovation fond Denmark, Grant No. 7038−00185B.

Notes

The authors declare the following competing financial interest(s): Christian V. Bertelsen and Gustav E. Skands are co-founders of SBT Instruments A/S and both own shares in the company.

ABBREVIATIONS

IFC, impedance flow cytometry; ROC, receiver operating characteristic; AUC, area under curve; PBS, phosphate buffered saline

REFERENCES

(1) Gawad, S.; Schild, L.; Renaud, P. Micromachined Impedance Spectroscopy Flow Cytometer for Cell Analysis and Particle Sizing. *Lab Chip* **2001**, *1* (1), 76−82.

(2) Morgan, H.; Sun, T.; Holmes, D.; Gawad, S.; Green, N. G. Single Cell Dielectric Spectroscopy. *J. Phys. D: Appl. Phys.* **2007**, *40* (1), 61−70.

(3) Xu, Y.; Xie, X.; Duan, Y.; Wang, L.; Cheng, Z.; Cheng, J. A Review of Impedance Measurements of Whole Cells. *Biosens. Bioelectron.* **2016**, *77*, 824−836.

(4) Spencer, D.; Morgan, H. High-Speed Single-Cell Dielectric Spectroscopy. *ACS Sens.* **2020**, *5* (2), 423−430.

(5) Honrado, C.; Ciuffreda, L.; Spencer, D.; Ranford-Cartwright, L.; Morgan, H. Dielectric Characterization of Plasmodium Falciparum-Infected Red Blood Cells Using Microfluidic Impedance Cytometry. *Journal of the Royal Society, Interface* **2018**, *15* (147), 20180416.

(6) De Ninno, A.; Errico, V.; Bertani, F. R.; Businaro, L.; Bisegna, P.; Caselli, F. Coplanar Electrode Microfluidic Chip Enabling Accurate Sheathless Impedance Cytometry. *Lab Chip* **2017**, *17* (6), 1158−1166.

(7) De Ninno, A.; Reale, R.; Giovinazzo, A.; Bertani, F. R.; Businaro, L.; Bisegna, P.; Matteucci, C.; Caselli, F. High-Throughput Label-Free Characterization of Viable, Necrotic and Apoptotic Human Lymphoma Cells in a Coplanar-Electrode Microfluidic Impedance Chip. *Biosens. Bioelectron.* **2020**, *150*, 111887.

(8) Heidmann, I.; Schade-Kampmann, G.; Lambalk, J.; Ottiger, M.; Di Berardino, M. Impedance Flow Cytometry: A Novel Technique in Pollen Analysis. *PLoS One* **2016**, *11* (11), No. e0165531.

(9) Canonge, J.; Philippot, M.; Leblanc, C.; Potin, P.; Bodin, M. Impedance Flow Cytometry Allows the Early Prediction of Embryo Yields in Wheat (Triticum Aestivum L.) Microspore Cultures. *Plant Science* **2020**, *300*, 110586.

(10) Clausen, C. H.; Skands, G. E.; Bertelsen, C. V.; Svendsen, W. E. Coplanar Electrode Layout Optimized for Increased Sensitivity for Electrical Impedance Spectroscopy. *Micromachines* **2015**, *6* (1), 110−120.

(11) Cottet, J.; Kehren, A.; van Lintel, H.; Buret, F.; Frénéa-Robin, M.; Renaud, P. How to Improve the Sensitivity of Coplanar Electrodes and Micro Channel Design in Electrical Impedance Flow Cytometry: A Study. *Microfluid. Nanofluid.* **2019**, *23* (1), 11.

(12) Zhang, X.; Wang, W.; Nordin, A. N.; Li, F.; Jang, S.; Voiculescu, I. The Influence of the Electrode Dimension on the Detection Sensitivity of Electric Cell-Substrate Impedance Sensing (ECIS) and Its Mathematical Modeling. *Sens. Actuators, B* **2017**, *247*, 780−790.

(13) Winkler, T. E.; Ben-Yoav, H.; Ghodssi, R. Hydrodynamic Focusing for Microfluidic Impedance Cytometry: A System Integration Study. *Microfluid. Nanofluid.* **2016**, *20* (9), 134.

(14) Grenvall, C.; Antfolk, C.; Bisgaard, C. Z.; Laurell, T. Two-Dimensional Acoustic Particle Focusing Enables Sheathless Chip Coulter Counter with Planar Electrode Configuration. *Lab Chip* **2014**, *14* (24), 4629−4637.

(15) Farooq, A.; Butt, N. Z.; Hassan, U. Exceedingly Sensitive Restructured Electrodes Design for Pathogen Morphology Detection Using Impedance Flow Cytometry. *2020 42nd Annual International Conference of the IEEE Engineering in Medicine Biology Society (EMBC)* **2020**, *2020*, 2500−2503.

(16) Clausen, C. H.; Dimaki, M.; Bertelsen, C. V.; Skands, G. E.; Rodriguez-Trujillo, R.; Thomsen, J. D.; Svendsen, W. E. Bacteria Detection and Differentiation Using Impedance Flow Cytometry. *Sensors (Switzerland)* **2018**, *18* (10), 3496.

(17) Haandbæk, N.; With, O.; Bürgel, S. C.; Heer, F.; Hierlemann, A. Resonance-Enhanced Microfluidic Impedance Cytometer for Detection of Single Bacteria. *Lab Chip* **2014**, *14* (17), 3313−3324.
(18) Bernabini, C.; Holmes, D.; Morgan, H. Micro-Impedance Cytometry for Detection and Analysis of Micron-Sized Particles and Bacteria. *Lab Chip* **2011**, *11* (3), 407−412.
(19) David, F.; Hebeisen, M.; Schade, G.; Franco-Lara, E.; Di Berardino, M. Viability and Membrane Potential Analysis of Bacillus Megaterium Cells by Impedance Flow Cytometry. *Biotechnol. Bioeng.* **2012**, *109* (2), 483−492.
(20) Di Berardino, M.; Hebeisen, M.; Hessler, T.; Ziswiler, A.; Largiadèr, S.; Schade, G. Impedance Microflow Cytometry for Viability Studies of Microorganisms. *Imaging, Manipulation, and Analysis of Biomolecules, Cells, and Tissues IX* **2011**, *7902*, 790212.
(21) Spencer, D. C.; Paton, T. F.; Mulroney, K. T.; Inglis, T. J. J.; Sutton, J. M.; Morgan, H. A Fast Impedance-Based Antimicrobial Susceptibility Test. *Nat. Commun.* **2020**, *11* (1), 5328.
(22) Bertelsen, C. V.; Franco, J. C.; Skands, G. E.; Dimaki, M.; Svendsen, W. E. Investigating the Use of Impedance Flow Cytometry for Classifying the Viability State of E. *Coli. Sensors* **2020**, *20* (21), 6339.
(23) Green, R. G.; Larson, W. P. Conductivity of Bacterial Cells. *Journal of Infectious Diseases* **1922**, *30* (5), 550−558.
(24) Cangelosi, G. A.; Meschke, J. S. Dead or Alive: Molecular Assessment of Microbial Viability. *Appl. Environ. Microbiol.* **2014**, *80*, 5884.
(25) Shehadul Islam, M.; Aryasomayajula, A.; Selvaganapathy, P. R. A Review on Macroscale and Microscale Cell Lysis Methods. *Micromachines* **2017**, *8* (3), 83.
(26) Cheung, K. C.; Berardino, M. D.; Schade-Kampmann, G.; Hebeisen, M.; Pierzchalski, A.; Bocsi, J.; Mittag, A.; Tárnok, A. Microfluidic Impedance-Based Flow Cytometry. *Cytometry Part A* **2010**, *77* (7), 648−666.
(27) Ostermann, M.; Sauter, A.; Xue, Y.; Birkeland, E.; Schoelermann, J.; Holst, B.; Cimpan, M. R. Label-Free Impedance Flow Cytometry for Nanotoxicity Screening. *Sci. Rep.* **2020**, *10* (1), 1−14.
(28) Mallén-Alberdi, M.; Vigués, N.; Mas, J.; Fernández-Sánchez, C.; Baldi, A. Impedance Spectral Fingerprint of E. Coli Cells on Interdigitated Electrodes: A New Approach for Label Free and Selective Detection. *Sensing and Bio-Sensing Research* **2016**, *7*, 100−106.
(29) Rhyner, M. N. The Coulter Principle for Analysis of Subvisible Particles in Protein Formulations. *AAPS J.* **2011**, *13* (1), 54−58.
(30) Asami, K.; Hanai, T.; Koizumi, N. Dielectric Approach to Suspensions of Ellipsoidal Particles Covered with a Shell in Particular Reference to Biological Cells. *Jpn. J. Appl. Phys.* **1980**, *19* (2), 359−365.
(31) Valero, A.; Braschler, T.; Renaud, P. A Unified Approach to Dielectric Single Cell Analysis: Impedance and Dielectrophoretic Force Spectroscopy. *Lab Chip* **2010**, *10* (17), 2216−2225.
(32) Stubbe, M.; Gimsa, J. Maxwell's Mixing Equation Revisited: Characteristic Impedance Equations for Ellipsoidal Cells. *Biophys. J.* **2015**, *109*, 15.
(33) Cottet, J.; Fabregue, O.; Berger, C.; Buret, F.; Renaud, P.; Frénéa-Robin, M. MyDEP: A New Computational Tool for Dielectric Modeling of Particles and Cells. *Biophys. J.* **2019**, *116* (1), 12−18.
(34) Gawad, S.; Cheung, K.; Seger, U.; Bertsch, A.; Renaud, P. Dielectric Spectroscopy in a Micromachined Flow Cytometer: Theoretical and Practical Considerations. *Lab Chip* **2004**, *4* (3), 241−251.
(35) Nanninga, N. Morphogenesis of Escherichia Coli. *Microbiol Mol. Biol. Rev.* **1998**, *62* (1), 110−129.
(36) Bai, W.; Zhao, K. S.; Asami, K. Dielectric Properties of E. Coli Cell as Simulated by the Three-Shell Spheroidal Model. *Biophys. Chem.* **2006**, *122* (2), 136−142.

https://doi.org/10.1021/acsomega.2c07357
ACS Omega 2023, 8, 7714−7721